Interference substructure of above-threshold ionization peaks in the stabilization regime

Koudai Toyota,[1] Oleg I. Tolstikhin,[2] Toru Morishita,[1,3] and Shinichi Watanabe[1]
[1]*Department of Applied Physics and Chemistry, University of Electro-Communications, 1-5-1, Chofu-ga-oka, Chofu-shi, Tokyo, Japan*
[2]*Russian Research Center "Kurchatov Institute," Kurchatov Square 1, Moscow 123182, Russia*
[3]*PRESTO, Japan Science and Technology Agency, Kawaguchi, Saitama 332-0012, Japan*
(Received 8 August 2008; published 29 September 2008)

The photoelectron spectra produced in the photodetachment of H^- (treated in the single-active-electron approximation) by strong high-frequency laser pulses with adequately chosen laser parameters in the stabilization regime are theoretically studied for elliptic polarization over an extended parameter range. An oscillating substructure in the above-threshold ionization peaks is observed, which confirms similar findings in the one-dimensional (1D) [K. Toyota *et al.*, Phys. Rev. A **76**, 043418 (2007)] and 3D calculations for linear polarization [O. I. Tolstikhin, Phys. Rev. A **77**, 032712 (2008)]. The mechanism is an interference between the photoelectron wave packets created in the rising and falling parts of the pulse which is specific to the stabilization regime. We thus conclude that this interference substructure is robust for any polarization and over a wide range of the laser parameters, and hence should be observable experimentally.

DOI: 10.1103/PhysRevA.78.033432 PACS number(s): 32.80.Rm, 31.15.−p, 31.70.Hq, 32.80.Fb

I. INTRODUCTION

Recent experimental developments in high-order-harmonic generation [1] and free-electron lasers [2,3] provide us with coherent light sources in the x-ray range, where the wavelength and intensity can reach up to tens of nanometers and $\sim 10^{14}$ W/cm^2, respectively [1]. Such new light sources experimentally opened up the so-called high-frequency regime, and revealed interesting dynamics of atoms and molecules [4–7]. Experimentalists may further aspire to develop an ultraintense laser pulse to reach the stabilization regime in future. Stabilization is a phenomenon in which the total ionization yield decreases once the laser intensity exceeds a certain critical value. It was first predicted by theory (see [8,9] for the history and detailed discussion of stabilization). However, as far as we know, theoretical studies in this regime usually concentrate on the ionization rate or total ionization probability (see, e.g., [10]; see also the review articles [11,12] and references therein). Such gross characteristics are important, but describe only one aspect of the dynamics. To gain insight into further details, it is essential to consider the photoelectron spectrum, which is a more sensitive characteristic and may bear various signatures of the dynamics not revealed by the total ionization probability. To provide a look at one general feature of the dynamics of ionization by laser pulses in the stabilization regime via analysis of the photoelectron spectra is one of the goals of this paper.

Even though seldom acknowledged explicitly, it is not straightforward to reliably calculate photoelectron spectra. Conventional methods based on zero boundary conditions or absorbing potentials lead to a spectrum contaminated by unphysical reflections from the boundary, so the resolution of the high-energy region is limited. This difficulty has been resolved in a recently developed Siegert-state expansion approach [13–16]. The Siegert states (SSs) are the solutions of the stationary Schrödinger equation which satisfy the outgoing-wave boundary condition. The idea was originally introduced by Siegert in 1939 [17]; more recently, Tolstikhin *et al.* [18] introduced Siegert pseudostates which became a powerful tool in practical calculations. The theory of SSs has been developed systematically in [19–22]. The SSs have already found many applications in atomic physics in the time-independent framework [23–28]. The use of SSs as a means to eliminate unphysical reflections from the boundary in time-dependent studies of stationary systems was initiated in [29–31]. Further extension of this approach to nonstationary systems [13–16] made its applications to the laser-atom interaction problem possible. One of the main advantages of the approach is that it enables one to accurately calculate photoelectron spectra with any desired resolution. This was demonstrated by calculations for model one-dimensional (1D) systems [14,32] and for linear polarization in the 3D case [16]. A demonstration of the SS expansion approach for elliptic polarization in the 3D case is another goal of this work.

In the 1D calculations [32], we found an oscillating substructure in the above-threshold ionization (ATI) [33] peaks produced in photoionization (or rather photodetachment) of the hydrogen negative ion H^- by strong high-frequency laser pulses. It was shown that this is due to an interference between photoelectron wave packets created in the rising and falling parts of the pulse and that stabilization plays a key role. Subsequently, the effect was confirmed by 3D calculations for linear polarization [16]. Here, we follow these previous papers but consider a general elliptic polarization and vary the laser parameters to show that our findings are robust. We give an interpretation of the effect in terms of an adiabatic version of the high-frequency Floquet theory (HFFT) [34]. Although this analysis is similar to that in [32], the generalization to the 3D case is not straightforward, and it is not evident *a priori* that such a simple approximation applies to the 3D case as well.

The paper is thus organized as follows. Section II recalls basic equations of our approach. In Sec. III, we present and discuss our numerical results for the photoelectron spectra from H^-—this system seems to be more easily amenable to the high-frequency strong-field regime of interest here. The oscillating substructure in the ATI peaks indeed appears in a

wide range of laser parameters. In Sec. IV, we interpret these results and reconstruct the oscillating substructure, if approximately, in terms of the HFFT. Section V concludes the paper. Atomic units are used throughout.

II. THEORETICAL APPROACH

We consider a negative hydrogen ion H^- interacting with a laser pulse. The ion is treated in the single-active-electron approximation. The time-dependent Schrödinger equation (TDSE) describing the system in the laboratory frame (L) in the length gauge reads

$$i\frac{\partial\psi_{\rm L}(\mathbf{r}_{\rm L},t)}{\partial t}=\left(-\frac{1}{2}\Delta_{\rm L}+V(r_{\rm L})+\mathbf{r}_{\rm L}\cdot\mathbf{F}(t)\right)\psi_{\rm L}(\mathbf{r}_{\rm L},t), \quad (1)$$

where $V(r)$ is the atomic potential and $\mathbf{F}(t)$ is the electric field. The potential is modeled by [16]

$$V(r)=-V_0\exp(-r^2/r_0^2) \quad (2)$$

with $V_0=0.383\,108\,7$ and $r_0=2.5026$. This potential supports only one bound state with energy $E_0=-0.027\,751\,0$ and is characterized by the s-wave scattering length 5.965, thus yielding accurate variational results for H^-. We have tried several soft-core model potentials with different asymptotic behavior; the results reported below only weakly depend on the model as long as the bound-state energy and (importantly) scattering length are reproduced correctly. The field $\mathbf{F}(t)$ is assumed to vanish beyond the time interval $0\leqslant t\leqslant T$. Let us introduce a classical trajectory of an electron moving under the influence of only the electric field,

$$\ddot{\boldsymbol{\alpha}}(t)=-\mathbf{F}(t), \quad (3a)$$

$$\dot{\boldsymbol{\alpha}}(0)=\boldsymbol{\alpha}(0)=\mathbf{0}, \quad (3b)$$

where the overdot denotes the derivative with respect to time. The Kramers-Henneberger (KH) transformation is defined by [35,36]

$$\mathbf{r}_{\rm L}=\mathbf{r}_{\rm KH}+\boldsymbol{\alpha}(t), \quad (4a)$$

$$\psi_{\rm L}(\mathbf{r}_{\rm L},t)=\exp\left(i\dot{\boldsymbol{\alpha}}(t)\cdot\mathbf{r}_{\rm L}-\frac{i}{2}\int_0^t\dot{\boldsymbol{\alpha}}^2(t')dt'\right)\psi_{\rm KH}(\mathbf{r}_{\rm KH},t). \quad (4b)$$

Substituting these equations into Eq. (1), one obtains the TDSE in the KH frame,

$$i\frac{\partial\psi_{\rm KH}(\mathbf{r}_{\rm KH},t)}{\partial t}=\left(-\frac{1}{2}\Delta_{\rm KH}+V(|\mathbf{r}_{\rm KH}+\boldsymbol{\alpha}(t)|)\right)\psi_{\rm KH}(\mathbf{r}_{\rm KH},t). \quad (5)$$

The transformed potential combines the effect of the atomic potential and the laser field and is called the KH potential. The interaction between the electron and the laser field is thus described by a quiver motion of the KH potential along the classical trajectory. An important advantage of this representation is that the KH potential is well localized within the bound of this quiver motion. Indeed, let a be the radius of the atomic potential, i.e., in numerical calculations one can set $V(r>a)=0$ without modifying the results; $a\approx 6$ for the present model (2). Then the KH potential in Eq. (5) vanishes for $r_{\rm KH}>R=a+\alpha$, where $\alpha=\max\alpha(t)$ is the maximum excursion amplitude of the classical trajectory as measured from the origin and $\alpha(t)=|\boldsymbol{\alpha}(t)|$. Vanishing of the potential in the TDSE beyond some radius is required for the application of the SS expansion approach [13–16], therefore the use of the KH frame is the representation of choice for this approach. We solve Eq. (5) using the procedure described in [16]. This procedure is rather simple in implementation for soft-core potentials; it is equally applicable to potentials with the Coulomb singularity at the origin, although the calculation of the matrix elements in this case is complicated by the quiver motion of the singularity. This method incorporates the outgoing-wave boundary condition exactly at $r_{\rm KH}=R$; therefore only a very limited spatial region $r_{\rm KH}\leqslant R$ is to be considered. Nevertheless, all the interactions are fully taken into account and the method is capable of producing accurate photoelectron spectra with any desired resolution. A true laser pulse must satisfy [10,11]

$$\dot{\boldsymbol{\alpha}}(T)=\boldsymbol{\alpha}(T)=0. \quad (6)$$

In this case the spectra in the L and KH frames coincide, which simplifies the calculations. In the following, conditions (6) are applied.

III. PHOTOELECTRON SPECTRA IN THE STABILIZATION REGIME

A. Laser pulse

For an elliptically polarized pulse, we assume that the polarization vector lies in the xz plane. The components of the electric field $\mathbf{F}(t)$ are represented by $(0\leqslant t\leqslant T)$

$$F_x(t)=\varepsilon F_0 f(t)\sin\omega t, \quad (7a)$$

$$F_z(t)=F_0 f(t)\cos\omega t, \quad (7b)$$

where ε, F_0, ω, and T are the ellipticity, amplitude, frequency, and duration of the pulse, respectively. The pulse envelope $f(t)$ is defined by

$$f(t)=\left(1-\frac{n_{\rm oc}^2-4}{n_{\rm oc}^2-1}\cos^2\frac{\pi t}{T}\right)\sin^2\frac{\pi t}{T}, \quad (8)$$

where $n_{\rm oc}=\omega T/2\pi$ is the number of optical cycles in the pulse. Equation (8) differs from a frequently used $\sin^2$ envelope by the factor in parentheses. This factor does not qualitatively modify the bell-like shape of the envelope and is introduced in order to satisfy conditions (6). Indeed, one can easily verify that for a pulse defined by Eqs. (7) and (8) with integer $n_{\rm oc}\geqslant 3$ Eqs. (6) hold for any value of ε.

In the following, we concentrate on a regime characterized by high frequencies $\omega\gg|E_0|$ and sufficiently large field amplitudes F_0 for stabilization to occur. Let us define the parameters of a reference laser pulse in this regime: $F_0=0.5$ $(I=cF_0^2/8\pi=8.8\times10^{15}\ \mathrm{W/cm^2})$, $\omega=\pi/10$ (8.55 eV), and $T=600$ (14.4 fs); hence $n_{\rm oc}=30$. The results reported be-

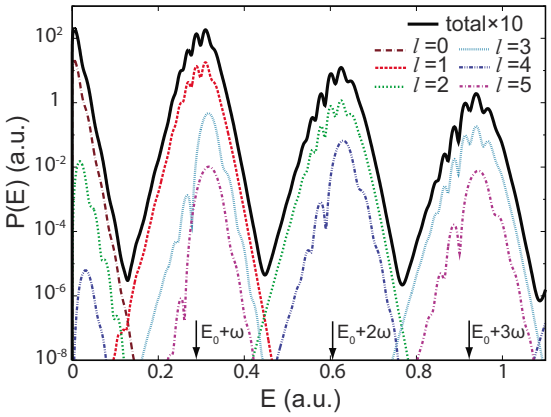

FIG. 1. (Color online) The partial wave and total photoelectron spectra for the reference laser pulse with the parameters $\varepsilon=1$, $F_0=0.5$, $\omega=\pi/10$, and $T=600$. The multiphoton absorption energies $E_0+n\omega$ are shown by arrows. Note that the total spectrum is multiplied by 10 to separate it from the other curves.

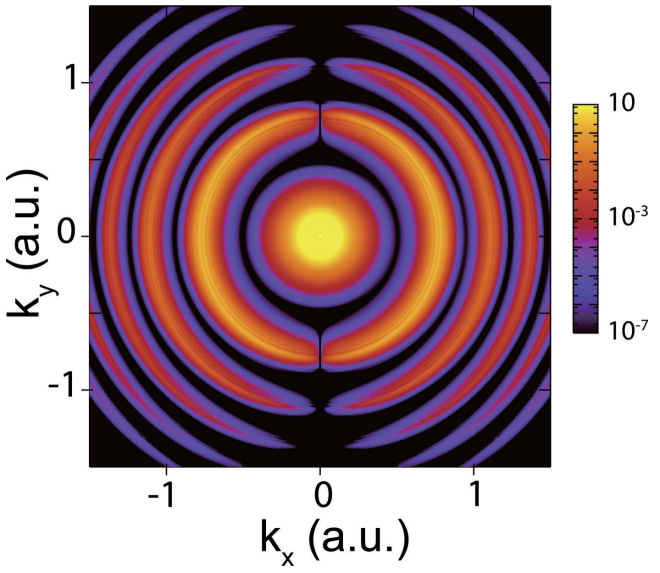

FIG. 2. (Color online) Momentum distribution of the photodetached electron in the xy plane for the same (circularly polarized in the xz plane) pulse as in Fig. 1.

low are obtained with the cutoff radius $R=12$ and the number of primitive radial basis functions used to construct the partial-wave Siegert pseudostates $N=40$ [16,22]. The maximum angular momentum included in the partial-wave expansion is $L=5$.

B. Numerical results

The general structure of the photoelectron spectrum in the stabilization regime is illustrated in Fig. 1. These results are obtained for the reference laser pulse with circular ($\varepsilon=1$) polarization. They look similar to those for the linear polarization case [16]. The partial-wave energy distributions are obtained by summing over the magnetic quantum number, and the total is the sum over all partial-waves. One can clearly see a train of ATI peaks [33] located around the n-photon absorption energies $E_0+n\omega$, $n=1,2,\ldots$. The peak associated with absorption of n photons will be called the nth peak. The nth ATI peak consists of the partial waves with angular momenta $l=n,n+2,n+4,\ldots$ of the same parity as n, with the dominant contribution coming from $l=n$. Thus, e.g., the first peak is dominated by the partial wave with $l=1$. This may seem to be a trivial consequence of the standard perturbation theory and dipole selection rule. However, the total ionization probability for the present pulse is 0.972, so the situation is very far from the perturbation regime. One can notice also a peak located at zero energy which is dominated by the partial wave with $l=0$; we shall call it the zeroth peak. The contribution of this peak to the total ionization probability is 0.263, so it represents a prominent feature that cannot be neglected. The zeroth peak arises from a quite different mechanism; its origin requires a separate discussion not congruous with the purpose of the present paper and is thus postponed till future. The contributions of higher partial waves to the total ionization probability are 0.637, 0.465×10^{-3}, 0.206×10^{-3}, 0.378×10^{-4}, and 0.108×10^{-4} for l from 1 through 5, respectively. Thus the partial-wave expansion rapidly converges.

A map of the 3D momentum distribution of the photodetached electron in the xy plane (perpendicular to the polarization plane xz) for the same pulse as in Fig. 1 is shown in Fig. 2. The bright disk at the center is the zeroth peak mentioned above. The series of bright rings correspond to the ATI peaks. For the present case of circular polarization the momentum distribution looks axially symmetric about the y axis (the direction of propagation of the laser pulse), although this symmetry is not exact. We recall that in the linear polarization case the distribution is exactly axially symmetric about the polarization axis [16]. The cut of ATI rings at $k_x=0$ reflects their partial wave contents in terms of the magnetic quantum number. It is explained by the fact that the dominant contribution to the nth peak comes from the partial wave with $l=n$ and the maximum projection of the angular momentum on the y axis. This feature is in accordance with the absorption of n circularly polarized photons and again may seem to be a trivial consequence of the standard perturbation theory in the L frame, although the situation is highly nonperturbative. In fact, we shall see below that the problem *can* be treated perturbatively, but this must be done in the KH frame within the HFFT [34].

An oscillatory substructure in ATI peaks is clearly seen in Fig. 1; it is also noticeable as ripples within ATI rings in Fig. 2. This substructure was first found in the 1D calculations [32]. It was shown to be due to an interference between photoelectron wave packets created in the rising and falling parts of the laser pulse [32]. A similar interference substructure is also found in the 3D calculations for linear polarization [16]. In the rest of the paper, we discuss this substructure and clarify the underlying interference mechanism, focusing on the first ATI peak. In doing so, we follow a train of thought similar to that in [16,32], but deal with circular and elliptic polarizations to show that the effect is robust for any polarization and under variations of the laser parameters.

First, we discuss the dependence of the spectrum on the field amplitude. We consider circularly polarized pulses with $\omega=\pi/10$ and $T=600$ and different values of F_0 (see Fig. 3).

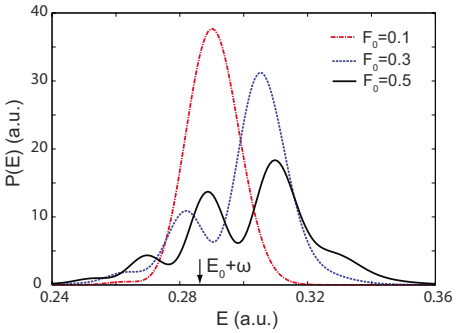

FIG. 3. (Color online) The first ATI peak for pulses with $\varepsilon=1$, $\omega=\pi/10$, and $T=600$ and three values of the field amplitude $F_0=0.1$, 0.3, and 0.5.

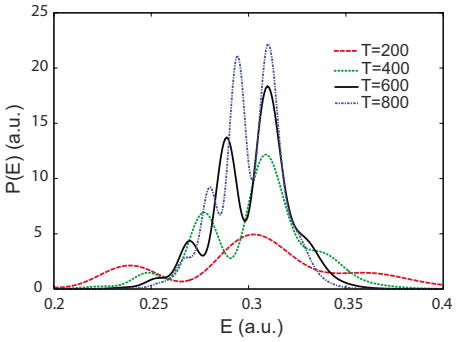

FIG. 4. (Color online) The first ATI peak for pulses with $\varepsilon=1$, $F_0=0.5$, and $\omega=\pi/10$ and four values of the duration of the pulse $T=200$, 400, 600, and 800.

The dynamics can be understood with the help of the classical trajectory $\boldsymbol{\alpha}(t)$. The maximum of the excursion amplitude $\alpha(t)$ for the pulse (7) is achieved somewhere near $t=T/2$ and can be estimated as $\alpha\approx F_0/\omega^2$. It is important to realize that there exists a critical amplitude α_c associated with the onset of stabilization. One may expect that the ionization rate $\Gamma(t)$ grows (decays) in the rising (falling) part of the pulse, because the electron becomes more loosely (tightly) bound as the excursion amplitude increases (decreases) with the variation of the field envelope. In this case, the function $\Gamma(t)$ has a bell-like shape centered at $t=T/2$; only a single photoelectron wave packet is created near the maximum of the pulse, and hence no interference substructure is expected to appear. This picture is correct for $\alpha<\alpha_c$. However, the situation is different for $\alpha>\alpha_c$. In this case, $\Gamma(t)$ first grows in the rising part of the pulse, in the interval $0\leqslant t\leqslant t_c$ where $\alpha(t)<\alpha_c$. When the excursion amplitude exceeds α_c, the electron behaves as almost free. It is well known that a free electron cannot absorb a photon. Hence $\Gamma(t)$ decays in the interval $t_c\leqslant t\leqslant T/2$, where the field envelope continues to rise and the excursion amplitude satisfies $\alpha(t)>\alpha_c$. This behavior is repeated in the inverse order in the falling part of the pulse: $\Gamma(t)$ first grows $(T/2\leqslant t\leqslant T-t_c)$ and then decays $(T-t_c\leqslant t\leqslant T)$. Thus the function $\Gamma(t)$ has two humps; hence two photoelectron wave packets are created whose interference may produce an oscillating substructure in the spectrum. As can be seen from Fig. 3, for $F_0=0.1$ the first ATI peak has a simple bell-like shape centered near the one-photon absorption energy $E_0+\omega$, as one would expect in the perturbation regime (for the present parameters $n_{\mathrm{oc}}=30$, so the pulse is rather monochromatic). However, a pronounced oscillating substructure appears for larger values of F_0. The threshold value of the field amplitude for which this substructure becomes clearly visible is estimated to be $F_0\approx 0.2$, which corresponds to $\alpha_c\approx 2$.

Second, we discuss the dependence of the spectrum on the duration of the pulse. We again consider circularly polarized pulses with $\omega=\pi/10$, with a fixed field amplitude $F_0=0.5$ and the different values of T (see Fig. 4). In these calculations $\alpha\approx 5.07$, which is definitely larger than α_c as estimated above. The interference substructure of the first ATI peak can be clearly seen in the figure. The frequency of the oscillations grows with T, because the interference phase is proportional to T as is shown below. However, the contrast of the fringes deteriorates as T grows. This is explained by the fact that for a good contrast the two interfering wave packets must have comparable amplitudes. Meanwhile, for too long pulses, complete depletion of the initial state occurs in the rising part of the pulse, so the amplitude of the second wave packet becomes much smaller than that of the first one.

Finally, we discuss the dependence of the spectrum on the laser polarization. We consider pulses with $F_0=0.5$, $\omega=\pi/10$, and $T=600$ for the polarization varying from linear $\varepsilon=0$ to circular $\varepsilon=1$ (see Fig. 5). In all cases, a pronounced oscillating substructure can be clearly seen. We thus conclude that this substructure is robust for all possible polarizations. The variance of the position of the interference fringes is due to the difference of the corresponding classical trajectories.

Summarizing, the range of the laser parameters for the interference substructure is identified as follows: (a) arbitrary polarization, (b) sufficiently high frequency, $\omega\gg|E_0|$, (c) sufficiently high intensity, $\alpha\approx F_0/\omega^2>\alpha_c$, and (d) a pulse length T not too small, to have at least a few fringes within the width of the ATI peak, but neither too large to have a good contrast.

IV. DISCUSSION OF THE INTERFERENCE MECHANISM

A. Numerical experiment: Adiabatic rotation of the polarization axis

The oscillating substructure discussed above results from an interference of the photoelectron wave packets created in

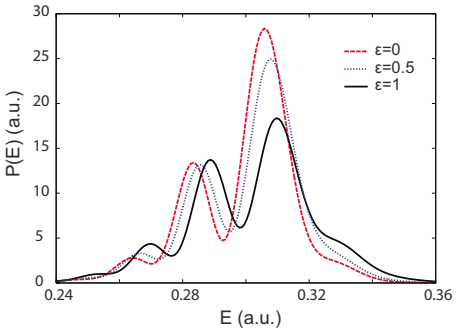

FIG. 5. (Color online) The first ATI peak for pulses with $F_0=0.5$, $\omega=\pi/10$, and $T=600$ with linear $(\varepsilon=0)$, intermediate elliptic $(\varepsilon=0.5)$, and circular $(\varepsilon=1)$ polarizations.

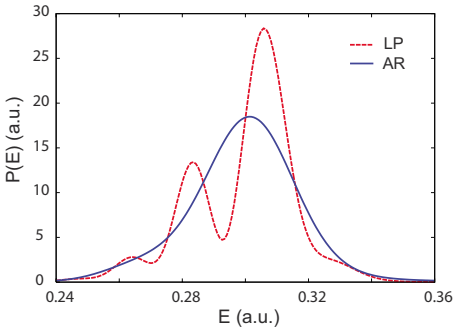

FIG. 6. (Color online) The first ATI peak for linear polarization (LP) along the z axis and in the case where the polarization axis is adiabatically rotated (AR) from z to x near the center of the pulse in order to suppress the interference (see text). The laser parameters are $F_0=0.5$, $\omega=\pi/10$, and $T=600$.

the rising and falling parts of the pulse. This does not provide yet an explanation of the physical mechanism, but suggests a basis on which a more detailed understanding of the dynamics can be constructed. In this section we discuss a numerical experiment which unambiguously confirms this basis. Let us consider a laser pulse defined by [cf. Eqs. (7)]

$$F_x(t) = [1 - s^2(t - T/2)]F_0 f(t)\cos\,\omega t, \tag{9a}$$

$$F_z(t) = s(t - T/2)F_0 f(t)\cos\,\omega t, \tag{9b}$$

where $f(t)$ is the envelope function (8) and $s(t)$ is a switching function which smoothly varies from 1 to 0 as t passes through zero in the positive direction. The effect of introducing the switching function is to adiabatically rotate the polarization axis from z to x within a few laser cycles near the center of the pulse, $t=T/2$. The photoelectron wave packets created in the rising and falling parts of the pulse in this case propagate in different directions, along the z and x axes, respectively. Hence they do not interfere and the oscillating substructure in the spectrum should not appear. Figure 6 compares the first ATI peak for linear polarization (LP), i.e., Eqs. (7) with $\varepsilon=0$, and in the case where the polarization axis is adiabatically rotated (AR), in the manner of Eqs. (9). The laser parameters in these calculations are $F_0=0.5$, $\omega=\pi/10$, and $T=600$. Indeed, one can see clear oscillations in the spectrum in the LP case, but none in the AR case. The AR spectrum reveals the true shape of each of the wave packets created and serves as a background for the oscillations in the LP spectrum. Thus, by rotating the polarization axis at a time between the two humps of the ionization rate $\Gamma(t)$, one can control the interference substructure. Whether this is feasible experimentally remains an open question.

B. Analysis in terms of the high-frequency Floquet theory

Having established the fact that the observed oscillations in the spectrum result from an interference mechanism, here we develop an approximate picture of the dynamics and reconstruct the first ATI peak using an adiabatic version of the HFFT [34]. The present analysis generalizes that of [32] to the 3D case. For definiteness, we consider a circularly polarized pulse [see Eqs. (7) with $\varepsilon=1$]. We shall treat the problem in the KH frame on the basis of Eq. (5). It is convenient to rotate the coordinate axes with respect to what has been implied in the above discussion in such a way that the polarization plane coincides with the xy plane, and thus the laser pulse propagates along the z axis. For brevity, in this section we omit the subscript KH in the notation of Eq. (5).

Let us consider a monochromatic laser field, i.e., we temporarily omit the envelope factor $f(t)$ in Eqs. (7). The classical trajectory in this case is given by $\boldsymbol{\alpha}(t)=(\alpha\cos\omega t,\alpha\sin\omega t,0)$, where $\alpha=F_0/\omega^2$ is the excursion amplitude. The KH potential can be expanded into a Fourier series,

$$V(|\mathbf{r}+\boldsymbol{\alpha}(t)|) = \sum_{n=-\infty}^{\infty} V_n(r,\theta;\alpha)e^{in(\varphi-\omega t)}, \tag{10}$$

where θ and φ are the polar angles defining the direction of $\mathbf{r}$. In the zeroth order of the HFFT [34], the system is described by the stationary "dressed" Hamiltonian

$$H_{\mathrm{HFFT}}(\alpha) = -\frac{1}{2}\Delta + V_0(r,\theta;\alpha). \tag{11}$$

It can be seen that $V_0(r,\theta;0)=V(r)$; hence $H_{\mathrm{HFFT}}(\alpha)$ reduces to the unperturbed atomic Hamiltonian in the absence of the field. The eigenfunctions of $H_{\mathrm{HFFT}}(\alpha)$ will be called the dressed states. Let $\psi_0(r,\theta;\alpha)$ and $E_0(\alpha)$ denote the eigenfunction and eigenvalue, respectively, of the initial bound dressed state, which coincides with the ground state of the unperturbed atom for $\alpha=0$. Let $\psi(\mathbf{r},\mathbf{k};\alpha)$ be the scattering dressed state corresponding to the momentum $\mathbf{k}=(k,\Omega)$ and energy $k^2/2$, normalized to unit amplitude of the incoming plane wave. Then, in the first order of the HFFT [34,37], the partial width of the initial state associated with the absorption of one photon is given by

$$\Gamma(\alpha) = \frac{k(\alpha)}{(2\pi)^2}\int |A(k(\alpha),\Omega;\alpha)|^2 d\Omega, \tag{12}$$

where $A(k,\Omega;\alpha)$ is the transition amplitude,

$$A(k,\Omega;\alpha) = \int \psi^*(\mathbf{r},\mathbf{k};\alpha)V_1(r,\theta;\alpha)e^{i\varphi}\psi_0(r,\theta;\alpha)d\mathbf{r}, \tag{13}$$

and $k(\alpha)$ is the momentum of the photoelectron,

$$k(\alpha) = \sqrt{2(E_0(\alpha)+\omega)}. \tag{14}$$

One can easily recognize in these formulas the first-order perturbation theory for the dressed interaction potential $V_1(r,\theta;\alpha)e^{i(\varphi-\omega t)}$ in the basis of the dressed states.

The coefficients $V_n(r,\theta;\alpha)$ in Eq. (10) can in turn be expanded in terms of the associated Legendre polynomials,

$$V_n(r,\theta;\alpha) = \sum_{l=n,n+2,\ldots} v_{nl}(r;\alpha)P_l^n(\cos\,\theta), \tag{15}$$

where the summation runs over l in steps of 2, since the left-hand side in Eq. (10) is an even function of $\cos\,\theta$. The

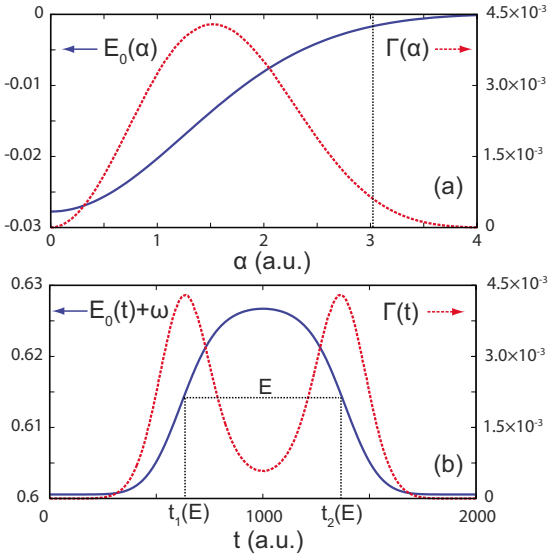

FIG. 7. (Color online) (a) Energy (solid line) and one-photon decay width (dashed line) of the initial dressed state as functions of the excursion amplitude $\alpha=F_0/\omega^2$ for $\omega=\pi/5$. (b) Same as in (a), but as functions of time recalculated using Eq. (18) for the laser pulse with $F_0=1.2$, $\omega=\pi/5$, and $T=2000$. The maximum value of $\alpha(t)$ for this pulse is shown by the vertical dotted line in the upper panel.

bound dressed state can be constructed numerically by substituting a partial-wave expansion,

$$\psi_0(r,\theta;\alpha)=\sum_{l=0,2,\ldots}\phi_l(r;\alpha)P_l(\cos\theta), \tag{16}$$

where, again, the summation runs only over even l since $\psi_0(r,\theta;\alpha)$ must be an even function of $\cos\theta$. Our calculations show that even for the largest excursion amplitude considered here, $\alpha=4$, the dressed binding potential $V_0(r,\theta;\alpha)$ preserves spherical symmetry to a good approximation, i.e., the term with $l=0$ in Eq. (15) dominates for $n=0$, and it is sufficient to retain only terms with $l=0$ and 2 in the expansion (16). The behavior of the eigenvalue $E_0(\alpha)$ is shown in Fig. 7(a). The initial state remains bound in the interval of α shown in the figure, but the binding energy monotonically decreases as α grows, since the potential $V_0(r,\theta;\alpha)$ becomes shallower. The scattering dressed state also can be constructed using a partial-wave expansion,

$$\psi(\mathbf{r},\mathbf{k};\alpha)=\sum_{lm}\phi_{lm}(r,\mathbf{k};\alpha)Y_{lm}(\theta,\varphi). \tag{17}$$

Only terms with $m=1$ contribute to the integral in Eq. (13). Our calculations show that in the expansion (15) for $V_1(r,\theta;\alpha)$ the term with $l=1$ dominates in the interval of α under consideration. This explains the results of the exact calculations discussed in Sec. III B: the dominant contribution to the first ATI peak comes from the partial wave with $l=1$ (see Fig. 1); the contribution from $l=3$ is smaller by an order of magnitude. Hence, to calculate $\Gamma(\alpha)$ it is sufficient to retain only the term with $(l,m)=(1,1)$ in the expansion (17). We approximately construct this term by retaining only the spherically symmetric part of the potential $V_0(r,\theta;\alpha)$.

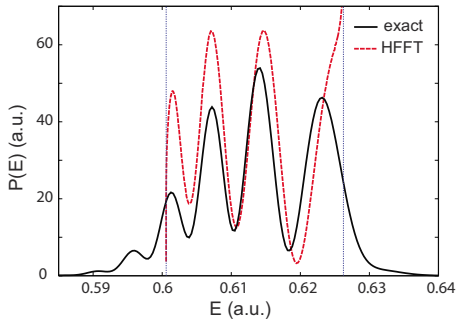

FIG. 8. (Color online) The first ATI peak for a circularly polarized laser pulse with $F_0=1.2$, $\omega=\pi/5$, and $T=2000$. The HFFT results are obtained from Eq. (22).

The dressed wave functions thus constructed are substituted into Eq. (13). The one-photon width of the initial state is obtained from Eq. (12). The error caused by the approximations made in this calculation is estimated to be within a few percent. The width $\Gamma(\alpha)$ calculated for $\omega=\pi/5$ is shown in Fig. 7(a). It first grows with α, but then decays after α passes the critical value $\alpha_c\approx 1.5$. This behavior of $\Gamma(\alpha)$, which is a signature of stabilization, is a key for understanding the ionization dynamics. To close this discussion, we note that the dominance of the $l=0$ and 1 components in the dressed binding $V_0(r,\theta;\alpha)$ and interaction $V_1(r,\theta;\alpha)$ potentials, respectively, means that the angular dependence of the transition amplitudes in the perturbation theory within the HFFT is similar to that in the standard perturbation theory in the L frame. However, the absolute values may be qualitatively different because of the effect of dressing on the initial and final states and the transition operator, as can be seen from the very fact of nonmonotonic behavior of $\Gamma(\alpha)$.

The remaining part of the analysis parallels that in [32]. To provide a clear illustration of our point, let us consider a laser pulse with the parameters $F_0=1.2$, $\omega=\pi/5$, and $T=2000$. The length of the pulse is increased compared to the previous cases, to have a pronounced interference substructure. The frequency is doubled, to keep a good contrast by reducing the decay rate. The field amplitude is increased accordingly to satisfy $\alpha>\alpha_c$. A part of the photoelectron spectrum near the first ATI peak ($E_0+\omega\approx 0.601$) calculated for this pulse is shown in Fig. 8. This pulse is not monochromatic. However, its envelope varies slowly; the pulse contains $n_{\mathrm{oc}}=200$ optical cycles. So one could expect that the picture suggested by the HFFT is followed adiabatically. The adiabatic approximation is implemented by the substitution

$$\alpha\to\alpha(t)=\frac{F_0}{\omega^2}f(t). \tag{18}$$

The maximum value of $\alpha(t)$ for the present parameters is $F_0/\omega^2=3.04$; it is shown by the vertical dotted line in Fig. 7(a). The behavior of $E_0(t)$ and $\Gamma(t)$, now as functions of t recalculated using the substitution Eq. (18), is shown in Fig. 7(b). The decay rate $\Gamma(t)$ indeed has two humps, as anticipated above. The probability to stay in the initial state until the moment t is, in this approximation,

$$P_0(t) \approx \exp\left(-\int_0^t \Gamma(t')dt'\right). \tag{19}$$

This gives $P_0(T) \approx 0.063$, which is not very far from the survival probability 0.055 obtained in our accurate calculations. Within the adiabatic approximation, the energy E of a photoelectron is a function of the moment t of its ionization,

$$E = E_0(t) + \omega \rightarrow t = t(E), \tag{20}$$

where $t(E)$ is the inverse function. The electrons ionized in the interval from t to $t+dt$ have energies between E and $E+dE$, where $dE=(dE_0(t)/dt)dt$. Equating the total ionization probability in this interval $P_0(t)\Gamma(t)dt$ to $C^2(E)|dE|$, where $C(E)$ is the amplitude of the photoelectron wave packet created, one finds

$$C(E) = \sqrt{P_0(t)\Gamma(t)\left|\frac{dt}{dE}\right|}\Bigg|_{t=t(E)}. \tag{21}$$

As can be seen from Fig. 7(b), for the present pulse $t(E)$ is a double-valued function. Let $t_1(E)$ and $t_2(E)$ denote its two branches, and $C_1(E)$ and $C_2(E)$ denote the corresponding amplitudes defined by Eq. (21). There are two different paths for the photoelectron with the energy E to evolve from $t=t_1(E)$ to $t=t_2(E)$. The first one is to be ionized at $t_1(E)$ and then propagate until $t_2(E)$ in the scattering state. The second one is to propagate between $t_1(E)$ and $t_2(E)$ in the bound state and then be ionized. These paths lead to the same final state, but with different phases. Summing up their contributions, the photoelectron spectrum is given by

$$P_{\mathrm{HFFT}}(E) = |C_1(E) + C_2(E)e^{i\Phi(E)}|^2, \tag{22}$$

where $\Phi(E)$ is the phase difference for the two paths,

$$\Phi(E) = E[t_2(E) - t_1(E)] - \int_{t_1(E)}^{t_2(E)} [E_0(t) + \omega]dt. \tag{23}$$

Note that for a fixed energy E this phase is proportional to the duration of the pulse T. The results obtained using these formulas are shown in Fig. 8. This approximate theory yields the spectrum only in a limited energy interval from $\min[E_0(t)+\omega]$ to $\max[E_0(t)+\omega]$, shown in the figure by vertical dotted lines. Equation (22) diverges at the upper boundary of this interval because of the factor $dt(E)/dE$ in Eq. (21). It nicely reproduces the phase of the interference substructure, but the amplitude is somewhat overestimated, especially in the lower part of the spectrum. However, in spite of these limitations, it is clear that the theory correctly accounts for the mechanism responsible for the appearance of the interference substructure. This analysis confirms our qualitative interpretation of the dynamics.

V. CONCLUSION

We discussed an interference effect in the dynamics of photoionization of atoms by strong high-frequency laser pulses in the stabilization regime. The effect was first found in 1D calculations [32] and then confirmed for linear polarization in the 3D case [16]. The present calculations show that it reveals itself for an arbitrary elliptic polarization and over a wide range of the laser parameters. Thus the effect is robust against variations of the laser parameters and should be observable experimentally. The accurate photoelectron spectra are calculated using the Siegert-state expansion approach [13–16]. An adiabatic version of the high-frequency Floquet theory [34] is developed to explain the interference mechanism. This approximate theory is confirmed by reconstructing the oscillating substructure of the first above-threshold ionization peak, which generalizes a similar analysis in [32] to the 3D case. The interference substructure discussed in [16,32] and in the present paper is a signature of the stabilization regime, sensitive to the details of the photoionization dynamics, so it could be used for probing the dynamics. The stabilization regime may soon become accessible by the rapidly developing light sources. Experimental certification of the stabilization effect is highly recommended.

The origin of the slow electrons represented by the zeroth peak in Fig. 1 and the bright disk at the center of Fig. 2 is different from the multiphoton absorption or from the interference mechanism discussed in this paper. Its explanation is expected to emerge on the basis of a recently developed theory of nonadiabatic transitions to the continuum [15]. We leave this issue for future studies.

ACKNOWLEDGMENTS

K.T. is partially supported by the Japan Society for the Promotion of Science (JSPS). O.I.T. gratefully acknowledges financial support from the Russian Science Support Foundation. This work is also supported in part by Grants-in-Aid for Scientific Research from the Ministry of Education, Culture, Sports, Science and Technology, Japan, and the 21st Century COE program on "Innovation in Coherent Optical Science," and by a JSPS Bilateral joint program between the U.S. and Japan.

[1] H. Mashiko, A. Suda, and K. Midorikawa, Opt. Lett. **29**, 1927 (2004).
[2] V. Ayvazyan *et al.*, Eur. Phys. J. D **37**, 297 (2006).
[3] G. Lambert *et al.*, Nat. Phys. **4**, 296 (2008).
[4] Y. Nabekawa, H. Hasegawa, E. J. Takahashi, and K. Midorikawa, Phys. Rev. Lett. **94**, 043001 (2005).
[5] T. Okino *et al.*, Chem. Phys. Lett. **432**, 68 (2006).
[6] R. Moshammer *et al.*, Phys. Rev. Lett. **98**, 203001 (2007).
[7] M. Nagasono *et al.*, Phys. Rev. A **75**, 051406(R) (2007).
[8] J. H. Eberly and K. C. Kulander, Science **262**, 1229 (1993).
[9] N. B. Delone and V. P. Krainov, Usp. Fiz. Nauk **165**, 1295 (1995) [Phys. Usp. **38**, 1247 (1995)].

[10] M. Boca, H. G. Muller, and M. Gavrila, J. Phys. B **37**, 147 (2004).
[11] M. Gavrila, J. Phys. B **35**, R147 (2002).
[12] A. M. Popov, O. V. Tikhonova, and E. A. Volkova, J. Phys. B **36**, R125 (2003).
[13] O. I. Tolstikhin, Phys. Rev. A **73**, 062705 (2006).
[14] O. I. Tolstikhin, Phys. Rev. A **74**, 042719 (2006).
[15] O. I. Tolstikhin, Phys. Rev. A **77**, 032711 (2008).
[16] O. I. Tolstikhin, Phys. Rev. A **77**, 032712 (2008).
[17] A. J. F. Siegert, Phys. Rev. **56**, 750 (1939).
[18] O. I. Tolstikhin, V. N. Ostrovsky, and H. Nakamura, Phys. Rev. Lett. **79**, 2026 (1997).
[19] O. I. Tolstikhin, V. N. Ostrovsky, and H. Nakamura, Phys. Rev. A **58**, 2077 (1998).
[20] G. V. Sitnikov and O. I. Tolstikhin, Phys. Rev. A **67**, 032714 (2003).
[21] K. Toyota, T. Morishita, and S. Watanabe, Phys. Rev. A **72**, 062718 (2005).
[22] P. A. Batishchev and O. I. Tolstikhin, Phys. Rev. A **75**, 062704 (2007).
[23] O. I. Tolstikhin, I. Yu. Tolstikhina, and C. Namba, Phys. Rev. A **60**, 4673 (1999).
[24] E. L. Hamilton and C. H. Greene, Phys. Rev. Lett. **89**, 263003 (2002).
[25] K. Toyota and S. Watanabe, Phys. Rev. A **68**, 062504 (2003).
[26] V. Kokoouline and C. H. Greene, Phys. Rev. Lett. **90**, 133201 (2003).
[27] G. V. Sitnikov and O. I. Tolstikhin, Phys. Rev. A **71**, 022708 (2005).
[28] R. Čurík and C. H. Greene, Phys. Rev. Lett. **98**, 173201 (2007).
[29] S. Yoshida, S. Watanabe, C. O. Reinhold, and J. Burgdörfer, Phys. Rev. A **60**, 1113 (1999).
[30] S. Tanabe, S. Watanabe, N. Sato, M. Matsuzawa, S. Yoshida, C. O. Reinhold, and J. Burgdörfer, Phys. Rev. A **63**, 052721 (2001).
[31] R. Santra, J. M. Shainline, and C. H. Greene, Phys. Rev. A **71**, 032703 (2005).
[32] K. Toyota, O. I. Tolstikhin, T. Morishita, and S. Watanabe, Phys. Rev. A **76**, 043418 (2007).
[33] P. Agostini, F. Fabre, G. Mainfray, G. Petite, and N. K. Rahman, Phys. Rev. Lett. **42**, 1127 (1979).
[34] M. Gavrila and J. Z. Kaminski, Phys. Rev. Lett. **52**, 613 (1984).
[35] H. A. Kramers, *Collected Scientific Papers* (North-Holland, Amsterdam, 1956), p. 272.
[36] W. C. Henneberger, Phys. Rev. Lett. **21**, 838 (1968).
[37] M. Marinescu and M. Gavrila, Phys. Rev. A **53**, 2513 (1996).